Rapid eITB Formation during Magnetic Shear Reversal in fully non-inductive TCV Discharges

M.A. Henderson, Y. Camenen, S. Coda, E. Fable, T.P. Goodman, P. Nikkola, A. Pochelon, O. Sauter, C. Zucca, and the TCV team

Centre de Recherches en Physique des Plasmas CRPP EPFL
Association EURATOM-Confédération Suisse
CH-1015 Lausanne, Switzerland

e-mail contact of the first author: Mark.Henderson@epfl.ch

Abstract. A rapid formation of an electron internal transport barrier (eITB) is observed during a slow evolution (~200ms) from a centrally peaked to a hollow current density profile, while all external actuators remain constant. The time constant for the barrier formation appears to be shorter than the electron energy confinement time. The improved confinement associated with the barrier formation occurs first in a localized region off-axis. Then the effects propagate to inner and outer flux surfaces on a confinement time scale. The temporal and spatial localization of the barrier formation suggest a threshold in the magnetic shear profile, which triggers the onset of the eITB. The location of the barrier corresponds to the radial location of the zero-shear flux surface based on a Fokker-Planck code and, therefore, we assume that the inversion of the q-profile corresponds to the barrier formation in both time and space. A simplified model is presented that attempts to characterize the current profile evolution and correlates the onset of the barrier with the time at which the current profile becomes inverted.

1. Introduction

Generation of non-inductively driven electron Internal Transport Barriers (eITB)[1,2,3,4] on the Tokamak à Configuration Variable (TCV) initially starts with a steady-state Ohmic plasma discharge with the current density profile (j_P) peaked in the center. The plasma current is then sustained using co-Electron Cyclotron Current Drive (ECCD) deposited off-axis (ρ_{CD}~0.4, 1.0MW), which broadens j_P. The co-ECCD current density profile (j_{CD}) is flat or slightly hollow from the deposition location inward due to a strong particle diffusion[5]. The off-axis co-ECCD also broadens and increases the electron temperature (T_e), steepening the electron pressure gradient off-axis (∇P_e) and resulting in an increased bootstrap current (I_{BS}). The bootstrap current density profile (j_{BS}) is peaked off-axis, and combines with j_{CD} to generate a slightly hollow j_P. The transition from a peaked to hollow j_P profile occurs on a slow time scale (~200ms). Even though the applied external loop voltage is zero, the plasma inductance generates local electric fields that drive internal currents (j_I), which attempt to maintain the peaked j_P profile that existed before the co-ECCD turn on. j_I decreases with a time constant τ_{jI},

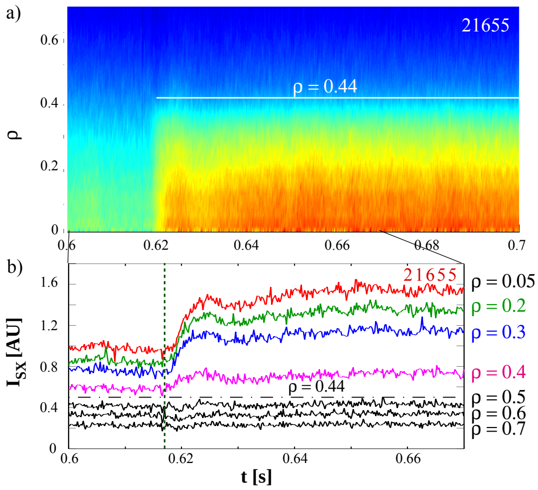

FIG. 1 a) The temporal evolution of the line-integrated soft x-ray emission across the plasma cross section, the eITB forms near 0.62s and b) viewed at selected values of ρ, during the eITB transition; the barrier foot position corresponds to the horizontal dashed-dotted line at ρ=0.44.[6]

governed by a combination of the current redistribution time and the plasma's L/R time constant. The transition from the centrally peaked to the hollow j_P is delayed until j_I is reduced to the point that it no longer fills in the hollow non-inductive current profile.

Despite the gradual evolution of the current profile and all external actuators being held constant, a rapid improvement in confinement is observed[6], see FIG. 1. The fast transition suggests the reaching of a threshold during the magnetic shear profile evolution, which triggers the onset of the eITB. We have determined the transition to occur at the moment at which the q profile becomes inverted. Unfortunately, there is no direct measurement of the local magnetic field line pitch angle on TCV, but simple modelling of the magnetic shear profile under equilibrium conditions and the of the current profile evolution, motivates the hypothesis that the rapid and localized barrier formation coincides with the appearance of the zero-shear (s=0) flux surface in time and space.

In the next section, the experimental evidence that the barrier forms rapidly and in a very localized region off-axis will be presented, with the position correlated to the modelled s=0 flux surface. Also, the formation of the barrier is shown to occur on an even faster time scale than the electron energy confinement time (τ_{eE}). In the third section a simplified model of the current profile evolution is presented, which approximates the three source current components: inductive, ECCD and bootstrap. The barrier's appearance is correlated with the inversion of the modelled current profile and the confinement enhancement is proportional to the modelled depth of the hollow j_P. Conclusions are offered at the end of this paper.

2. Spatial and temporal formation of the barrier

A typical eITB discharge from the turn on of the ECCD to a nearly steady state regime is shown in FIG. 2. The co-ECCD (1.0MW) is initiated at 0.4s, and at 0.42s all external actuators (including the ohmic transformer current, I_{OH}) are held constant. After 0.42s the plasma current is sustained by only I_{CD}, I_{BS} and I_I, and evolves from a peaked to hollow current profile as I_I decays on τ_{jI} scale. Approximately 200ms after the I_{OH} is held constant, a transition to the improved confinement regime is observed between 0.6 and 0.65s by the increase in the central electron temperature (T_{e0}), the electron energy confinement time (τ_{eE}) and the confinement enhancement factor, H_{RLW} ($=\tau_{eE}/\tau_{RLW}$)[7,8], see FIG. 2. Unfortunately, T_e and τ_{eE} are obtained on the Thomson Scattering (TS) diagnostic acquisition rate of 20Hz and can not resolve the rapid barrier formation evidenced by the soft x-ray emission (measured by a multiwire chamber proportional x-ray detector, MPX) of FIG. 1 and 2c, which occurs at t_T~0.618s. The barrier formation improves the confinement in the center as the emission from inner chords relative to ρ=0.44 increases, while the outer viewing chords register a momentary decrease as the barrier reduces the energy flux from the core to the outside, see FIG. 1b. The median radial location between the chords

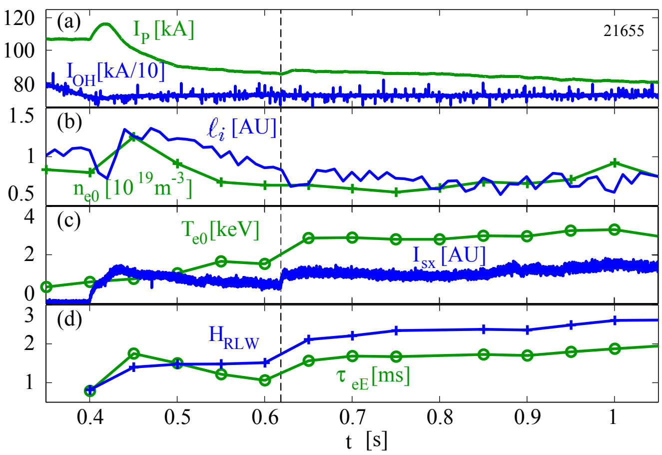

FIG. 2. *Typical eITB discharge with the improved confinement starting at 0.62s, including a) ohmic transformer coil current and plasma current; b) internal inductance and central electron density; c) I_{SX} and central T_e, and d) H_{RLW} and τ_{eE}..*

along which the emission respectively the increases and decreases corresponds to the barrier foot location, defined as the radial location of the maximum in ρ^*_T[9], which we refer to as ρ_{ρ^*}[10] (dashed line of FIG. 1b). The ρ^*_T parameter is defined as:

$$\rho^*_T = \rho_s / L_{Te}$$

where $L_{Te}=-T_e/(\partial T_e/\partial r)$ is the local temperature gradient scale length, $\rho_s=c_s/\omega_{ci}$ is the ion Larmor radius at the sound speed c_s ω_{ci} is the ion cyclotron angular frequency. After its inception the barrier's radial location remains stable until additional heating or counter-ECCD is applied in the center at 1.1s (not shown).

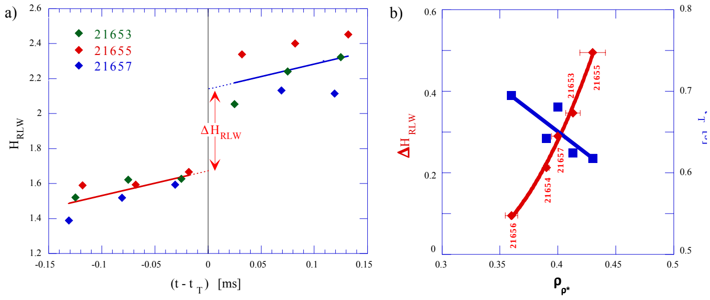

FIG. 3 a) The enhancement factor, H_{RLW} versus the time relative to the eITB formation time, t_T, for three different discharges. b) The step in confinement enhancement at t_T is correlated with the radial location (red curve) of the barrier formation. The time t_T (blue curve) is earlier for broader barriers.

Even though H_{RLW} is calculated on the TS acquisition rate, the rapid transition can also be observed by assembling several similar shots and plotting H_{RLW} at each TS acquisition time relative to t_T, see FIG. 3a. A gradual improvement in confinement is observed leading up to t_T, and then a rapid increase in H_{RLW} of magnitude ΔH_{RLW} occurs. There is a slight variation in ΔH_{RLW} for the three discharges, which can be attributed to the formation of the barrier at slightly different radial locations from shot-to-shot. If the barrier forms at a larger radius, the whole volume inside that radius will experience the improved confinement resulting in a greater step in ΔH_{RLW} as shown in FIG. 3b. It appears that ΔH_{RLW} depends on $\rho_{\rho^*}^2$ (proportional to the enclosed volume) as shown in FIG. 3b (red curve), consistent with the eITB figure of merit proposed in reference [10].

The chord-integrated I_{SX} seems to indicate a uniform increase across the whole core; however, chords viewing the plasma axis cannot distinguish between an increase at the center and an increase near the barrier. A recently upgraded MPX camera, viewing the entire plasma cross section, is used to obtain a local emissivity profile (ε_{SX}) by inverting the integrated profile, assuming a constant emissivity on a given flux surface and using a minimum Fisher inversion method[11]. The inverted profiles, averaged over 0.25ms and plotted at 0.75ms time intervals, are shown in FIG. 4a. The relative intensity (normalized to pre-eITB levels) for selected radial locations may then be plotted as a function of time, see FIG. 4b. An increase in the soft x-ray emission is first observed in the region of ρ~0.3, then progresses inward toward the center and outward toward the barrier foot. We chose to estimate the propagation time by fitting (solid line) the relative intensity change at each radial position to a hyperbolic tangent: $\varepsilon_{SX}(\rho)$ =

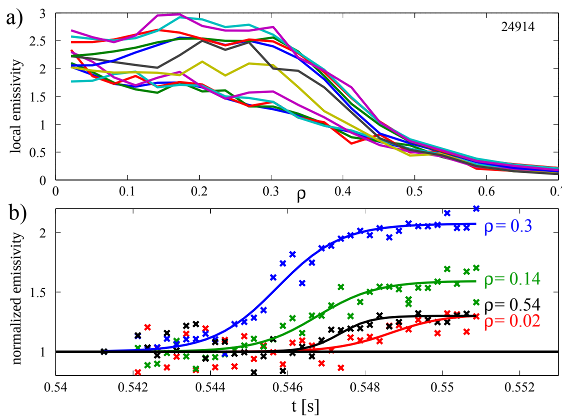

FIG. 4 a) The reconstructed ε_{SX} profiles averaged over 0.25s and plotted every 0.75ms during the eITB transition. b) The temporal evolution of ε_{SX} normalized and plotted for selected radial locations. The barrier forms first around ρ~0.3.

$\tanh[(t-t_T(\rho))/\tau_F(\rho)]$, where $\varepsilon_{SX}(\rho)$ corresponds to the amplitude rise, $t_T(\rho)$ the inflection point of the rise and $\tau_F(\rho)$ the rise time for the given flux surface ρ. The time of the initial rise of $\varepsilon_{SX}(\rho)$ at each radial location is approximated by $t_T(\rho)$-$\tau_F(\rho)$ and is plotted as a function of ρ in FIG. 5a. The increase in $\varepsilon_{SX}(\rho)$ occurs first at ρ~0.3, which can be attributed to a local decrease in thermal diffusivity, i.e. the formation of a barrier. As time progresses, neighbouring flux surfaces are influenced as the barrier "dams" the thermal flux resulting in a build-up of the local temperature. The inward and outward propagating effects of the barrier formation of FIG. 5a result in a relatively sharp "V" rather than a "U" shape indicating that the barrier width is very narrow (~0.05 in ρ or 1.2cm). The flat T_e profiles typical of the region contained inside eITBs[2,12] also indicate that the diffusivity is comparably higher inside ρ <0.3 than at the barrier. The barrier is located at the edge of the ε_{SX} or T_e flat top and not farther out at ρ_{ITB}[13] near the barrier foot (ρ=0.44 of FIG. 1b) characterized by the radial location of unchanging I_{SX}-chords.

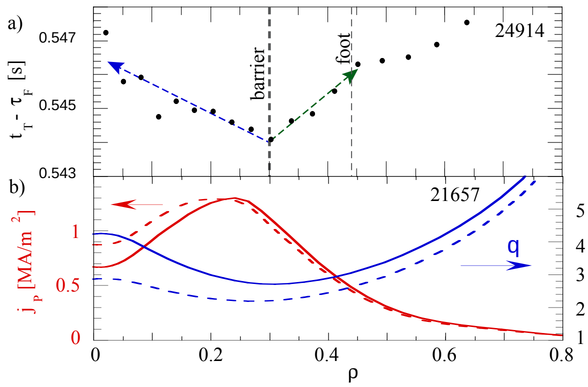

FIG 5 a) The fitted rise time (t_T-τ_F) of ε_{SX}: the barrier forms at ρ~0.3 (vertical dashed line) and the effects then propagate inward (blue line) and outward (green line). b) Calculated j_P and q-profile from the CQL3D code for shot #21657 (equivalent to #21655 and 24914 but in equilibrium conditions).

The j_P (red curves) and q profiles (blue curves) of FIG. 5b were calculated using the Fokker-Planck code, CQL3D[14] for an equivalent shot (#21657) after steady-state conditions were achieved. The calculations assumed two different averaged effective charge values, Z_{eff}=5 (solid) and 2.5 (dashed). In each case the diffusion coefficient (D) was chosen in such a way as to best reproduce the experimental total plasma current, *e.g.* D=0.5 m^2/s (solid) and 0.7 m^2/s (dashed)[15]. In both cases the zero-shear (*s*=0) flux surface occurs near ρ~0.3, equivalent to the barrier location ρ_B~0.3 of FIG. 5a. Since the barrier location corresponds to the modelled *s*=0 and the barrier position remains stable, it is reasonable to hypothesize that the threshold, which triggers the barrier formation, corresponds to the appearance of a zero-shear magnetic flux surface[6], i.e. that the barrier forms when and where *s*=0.

The step in confinement enhancement from the rise on the soft x-ray emission of FIG. 1 appears to occur on the order of τ_{eE}. However, if the transition occurred instantaneously, the increase in stored energy would occur on a similar τ_{eE} time scale, indicating that the formation of the barrier may occur at an even faster rate. In order to discern the formation speed, the confinement improvement is modelled as a function of time and of the barrier's formation time constant τ_F as follows:

$$\tau_{eE}(t) = \tau_{eE0} + \Delta\tau_{eE}\,(1+\tanh((t-\tau_F)/\,\tau_F))$$

where τ_{eE0} represents the initial global confinement time and $\Delta\tau_{eE}$ is the corresponding step associated with the onset of the eITB. The experimentally measured values are used for both τ_{eE0} and $\Delta\tau_{eE}$. The corresponding increase in the local soft x-ray emission can then be modelled as follows:

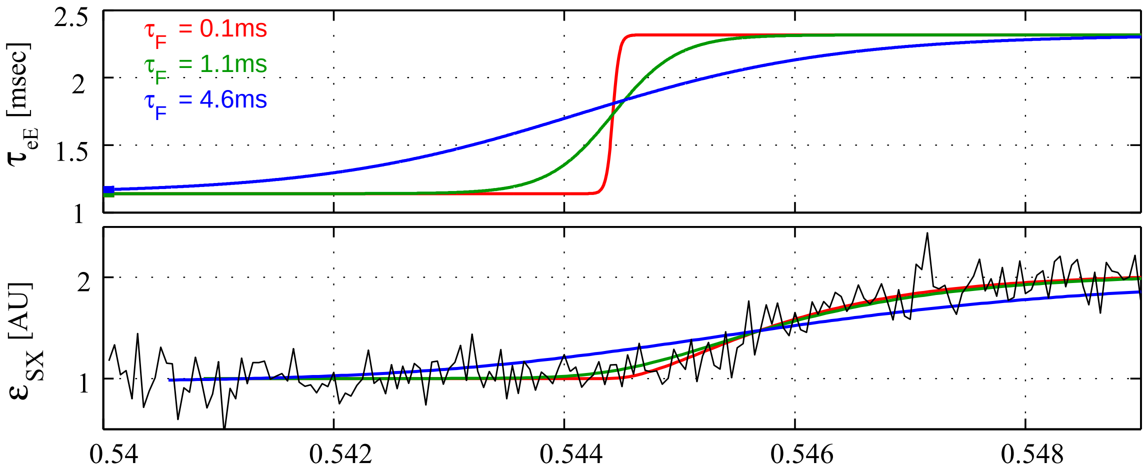

***FIG. 6** a) the modelled step in confinement at τ_F with the three chosen transition times $\tau_F=\tau_{eE}/20$ (red), τ_{eE} (green) and $4\tau_{eE}$ (blue). b) The modelled local soft x-ray emissivity for the three choices of τ_{eE} is compared to the experimental reconstructed local soft x-ray (black).*

$$\varepsilon_{mod}(t) = \frac{1}{\tau_n} \sum_{t_i=0}^{t} \varepsilon_0 \, e^{-(t-t_i)/\tau_{eE}(t_i)}$$

where ε_{mod} is the soft x-ray emission, ε_0 is the normalized reconstructed local emissivity, τ_n is a normilization factor and t_i is the interval time step chosen to be small relative to the confinement time scale ($t_i \ll \tau_{eE} \ll t$). An example of three barrier formation rates: $\tau_F = \tau_{eE}/20$ (red), $\tau_F = \tau_{eE}$ (green) and $\tau_F = 4\tau_{eE}$, are shown in FIG. 6a, with the corresponding modelled response in FIG. 6b along with the reconstructed local emissivity at ρ=0.3. The formation speed, can be estimated by choosing the value of τ_F that minimized the difference between ε_{mod} and ε_{SX} (Exp.). This was performed for each radial location of the reconstructed emissivity profiles. In the region near the barrier formation, τ_F <0.2ms (or $<\tau_{eE}/10$), which is nearly three orders of magnitude faster than the current evolution time scale τ_I. Note that the resolution of τ_F is limited to the MPX acquisition rate for this discharge (20kHz).

3. Current profile evolution

Since no direct measurement of the local magnetic field line pitch angle exists on TCV, we can only attempt to estimate the current density profiles through calculated and modelled profiles of the different source currents. After the current in the transformer coil is held constant, the plasma current is maintained by the sum of I_{CD} (net co-ECCD current), I_{BS} (net bootstrap current) and I_I (net current from the induced electric fields from the plasma inductance). I_{BS} can be calculated from the T_e and n_e profiles[16], and the time evolution of I_{CD} and I_I can be approximated using the following expression:

$$I_P(t) - I_{BS}(t) = c_1 \frac{T_e(\rho_{CD}, t)}{n_e(\rho CD, t)} + c_2 e^{-\frac{(t-0.42s)}{\tau_{jI}}}$$

where the first term represents the EC driven current (I_{CD}) and the second term the inductively induced currents that decay on a τ_{jI} scale. I_P is the measured total plasma current, and ρ_{CD} is the co-ECCD deposition location. The constants c_1, c_2 along with τ_{jI} are obtained from an optimization routine that minimizes the difference between the measured and modelled currents. The evolution of the measured, calculated and modelled sources is shown in FIG. 7a for a similar discharge (#21654). At 1.1s central heating is added which increases the central

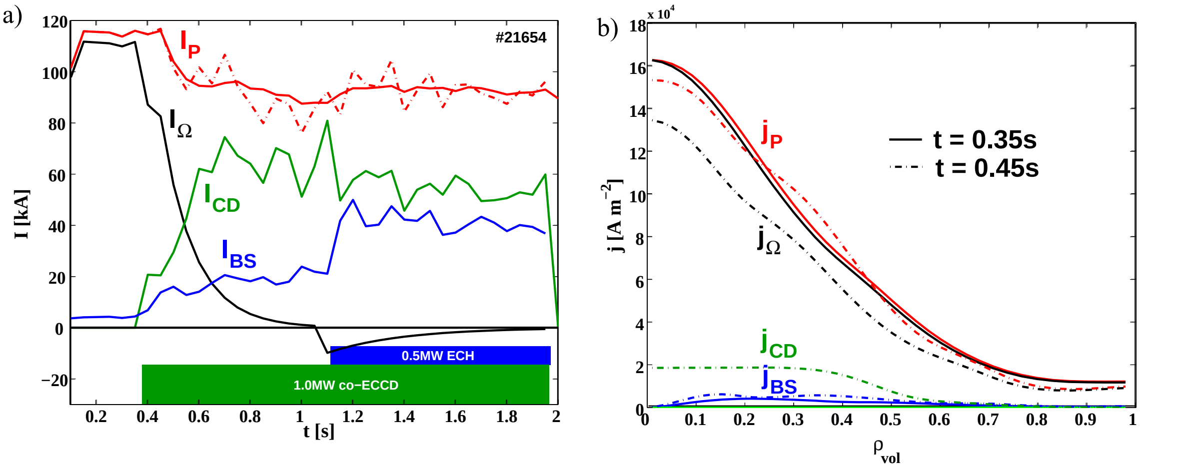

FIG. 7 a) Time evolution of the plasma current compared with the modelled contributions of I_{BS} (blue), I_{CD} (green), $I_\Omega + I_I$ (black) and their sum (red-dashed). b) The reconstructed current density profiles before and after the current in the transformer coil is held constant.

temperature, steepening the pressure gradient and increasing the driven bootstrap current. Again, the inductive nature of the plasma prevents rapid changes in the current profile, and a negative I_I is driven by the internal electric fields that then decay in time. The above minimization procedure is repeated during the central heated phase as shown in FIG. 7a. Once the magnitudes of the different current sources have been determined, the current density profiles can then be reconstructed. The profile shape of j_{CD}[15] is supplied by CQL3D, j_I at t=0.42s can then be calculated by subtracting (j_{CD}+j_{BS}) at t=0.42s+δ (where δ is a small time step) from j_{BS}+j_Ω at t=0.42s-δ, see FIG. 7b. Note that j_Ω is taken to be proportional to $T_e^{3/2}$, with the absolute amplitude constrained by the measured total current. Finally we can write $j_I = j_I(\rho)*e^{-(t-0.42)/\tau jI}$ from t=0.42 to 1.1s, and at 1.1s the process is repeated to obtain the complete profile evolution throughout the discharge. The modelled j_P becomes hollow between 0.6 and 0.65s consistent with the barrier formation near 0.64s (for #21654), see FIG. 8a. Although this is a simplified model of the complex evolution of j_P, the transition from a peaked to a hollow modelled j_P occurs consistently near the formation of the barrier for the five discharges analyzed. Hence it is reasonable to infer that the barrier forms once an *s*=0 surface appears in the plasma, which occurs soon after the j_P profile is inverted[6].

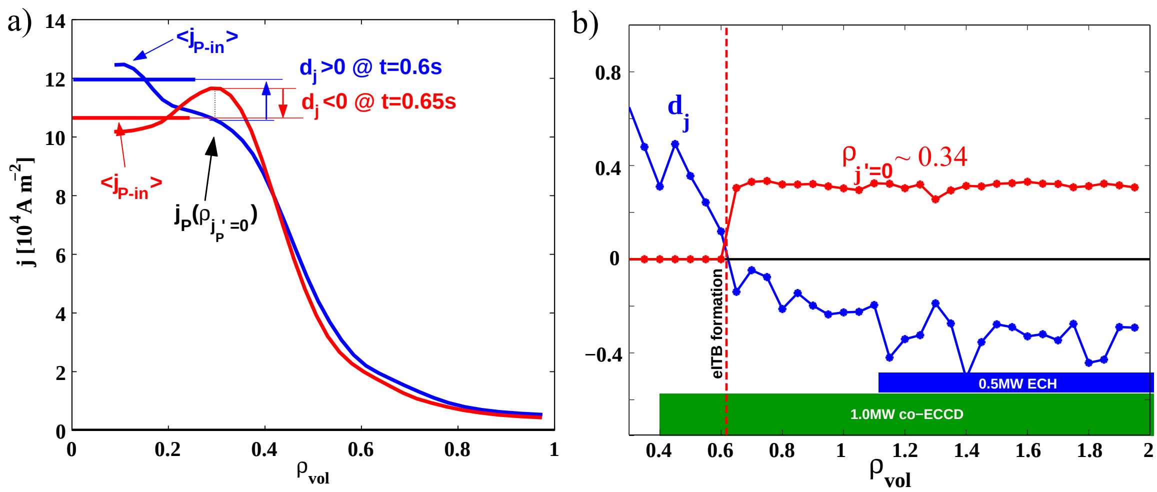

FIG. 8 a) Reconstructed j_P at the nearest TS acquisition time before (blue) and after (red) the barrier formation at t_T. b) The temporal evolution of d_j (height or depth of current center) during discharge #21654. t_T is represented by the red vertical dashed-line.

The depth of the hollow current profile can be characterized by $d_j = (j_{P\text{-}in} - j_{P\text{-}B}) / j_{P\text{-}B}$, where $j_{P\text{-}in}$ is the average current density inside $\rho = \rho_{jp'=0}$ (the radial location of the off axis maximum in j_P) and $j_{P\text{-}B}$ is the local current density at $\rho = \rho_{jp'=0}$. The evolution of both d_j and $\rho_{jp'=0}$ is shown in FIG. 8b, where the eITB transition occurs when d_j becomes negative. Note that the modelled j_P is strongly affected by the fluctuations in the T_e measurements, which provide the estimated j_{CD} and j_{BS} profiles. The average value of d_j was calculated for each discharge of FIG. 3b between 0.8 and 1.1s and plotted against the average maximum of ρ^* (referred to as the barrier strength, ρ^*_{max}), see FIG. 9. The results suggest a threshold in improved confinement once $d_j<0$ as well as when $\rho^*_{max}>0.04$[10]. The results further suggest that the improved confinement increases as the current profile (and q-profile) becomes more hollow (i.e. more inverted). However, the barrier width does not increase in size (as would be expected if the confinement increases with negative shear, but appears to remains relatively narrow at the zero shear flux surface. Therefore, the local improved confinement associated with the barrier improves with increasing d*s*/dr at the zero shear flux surface.

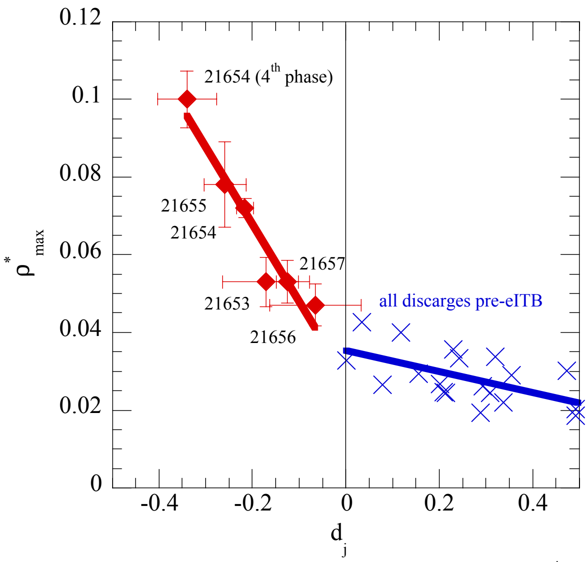

FIG. 9 *Comparison of the barrier strength, ρ^*_{max} versus d_j averaged after the barrier formation (red) and at each TS acquisition time before the transition (blue) for the same discharges of FIG. 3b.*

4. Conclusions

In conclusion, a rapid and localized formation of an internal transport barrier is observed during a slow evolution of the current density profile. The current profile evolution occurs on a relatively slow time scale, >200ms, from a well-defined peaked inductive ohmic profile to a steady-state fully non-inductively sustained hollow profile while all external actuators are held constant. The magnetic shear evolves on a similar time scale from a monotonically increasing to inverted profile. During this evolution, an internal transport barrier forms rapidly (<0.2ms) in a very narrow region off-axis. The barrier remains relatively stable at this location and the confinement improvement increases with the volume enclosed within the improved confinement region.

The barrier position is correlated to the zero shear flux surface according to the q profile modelled with CQL3D. A simplified model of the current profile evolution estimates the inversion of the current profile to occur when the barrier forms. The combination of the two models supports the hypothesis that the barrier forms when and where a zero shear flux surface appears[6]. The barrier strength, which is characterized as the maximum in the ρ^*_T parameter, increases linearly with the depth of the modelled current, implying that the barrier strength could be roughly proportional to d*s*/dr at the zero-shear flux surface. Here we have not invoked anything other than a local increase in confinement at a radial position corresponding to *s*=0 to explain the experimental data. The dual aspects of a rapid localized formation of the barrier at the modelled zero-shear flux surface and the barrier strength dependence on the d*s*/dr have yet to be incorporated in a single theory on internal transport barriers.

Acknowledgement:

The authors would like to acknowledge Basil Duval who helped greatly in proof reading and in numerous discussions concerning the organization of this manuscript. Also, Roland Behn and Ge Zhuang are to be acknowledged for their work with the Thomson Scattering diagnostic and Alexei Sushkov for his work with the MPX soft x-ray diagnostic. This work was partially supported by the Swiss National Science Foundation

Appendix 1: References

[1] S. Coda *et al*, "High-power ECH and fully non-inductive operation with ECCD in the TCV tokamak", Plasma Phys. Control. Fusion **42** (2000) B311.

[2] O. Sauter *et al*, "Electron ITB in fully non-inductive reverse shear scenarios", Proc. 29th EPS Conf. on Controlled Fusion and Plasma Physics (Montreux, 2002), Europhysics Conf. Abstr. **26B** (2002) P2-087.

[3] T.P. Goodman *et al*, "An overview of results from the TCV tokamak", Nucl. Fusion **43** (2003) 1619.

[4] M.A. Henderson *et al*, "Recent results from the electron cyclotron heated plasmas in Tokamak à configuration Variable (TCV)", Phys. Plasmas **10** (2003) 1796.

[5] P. Nikkola *et al*, "Modelling of the electron cyclotron current drive experiments in the TCV tokamak", Nucl. Fusion **43** (2003) 1343.

[6] M.A. Henderson *et al*, "Rapid and localized eITB formation during shear inversion in fully non-inductive TCV discharges", to be published in Phys. Rev. Lett (2004).

[7] P.H. Rebut, P.P. Lallia and M.L. Watkins, "The critical temperature gradient model of plasma transport: Applications to JET and future tokamaks", Proc. 12th Int. Conf. of Plasma Phys. and Cont. Fusion Res., **2** (IAEA, Vienna, 1989) p.191.

[8] A. Pochelon *et al*, "Energy confinement and MHD activity in shaped TCV plasmas with localized electron cyclotron heating", Nucl. Fusion **39** (1999) 1807.

[9] G. Tresset *et al*, "A dimensionless criterion for characterizing internal transport barriers in JET", Nucl. Fusion **42** (2002) 520.

[10] M.A. Henderson *et al*, "Control of electron internal transport barriers in TCV", Plasma Phys. Control. Fusion **46** (2004) A275.

[11] M. Anton *et al*, "X-ray tomography on the TCV tokamak", Plasma Phys. Control. Fusion **38** (1996) 1849.

[12] T. Fujita *et al*, "High performance experiments in JT-60U reversed shear discharges",Nucl. Fusion **39** (1999) 1627.

[13] B. Esposito *et al*, "JET internal transport barriers: experiment vs theory", Plasma Phys. Control. Fusion **45** (2003) 933.

[14] R.W. Harvey and M.G. McCoy, "The Fokker-Planck CQL3D code" in *Proceedings of the IAEA Technical Committee Meeting on Numerical Modeling of Plasmas, Montreal*, 1992 (IAEA, Vienna, 1993).

[15] P. Nikkola, "The effect of electron transport on electron cyclotron current drive in tokamak plasmas", EPFL Thesis No. 3048 (2004).

[16] O. Sauter, C. Angioni and Y.R. Lin-Liu, "Neoclassical conductivity and bootstrap current formulas for general axisymmetric equilibria and arbitrary collisionality regime", Phys. Plasmas **6** (1999) 2834.